Factorial Optimization of the Effects of Extrusion Temperature Profile and Polymer Grade on As-Spun Aliphatic–Aromatic Copolyester Fibers. II. Crystallographic Order

Basel Younes, Alex Fotheringham

Biomedical Textiles Research Centre (BTRC), Heriot-Watt University, School of Textiles and Design, Scottish Borders Campus, Netherdale, Galashiels, TD1 3HF, United Kingdom

Received 3 December 2009; accepted 31 May 2010
DOI 10.1002/app.32906
Published online 23 August 2010 in Wiley Online Library (wileyonlinelibrary.com).

ABSTRACT: By using factorial experimental design, a range of crystallographic orders for as-spun linear aliphatic–aromatic copolyester fibers have been characterized with the aid of wide angle X-ray diffraction measurements. Full-Width Half-Maximum of an X-ray scattering profile (FWHM) has been quantitatively assessed as responses to polymer grades denoted by melt flow index (MFI) and to extrusion temperature zones in the extrusion equipment used to produce the as-spun fibers. With the advantages of the factorial experimental design in the development of fiber process technology, the enhanced statistical approach specifies the direction of change of the polymer's melt flow index and extrusion temperature profile for increasing or reducing crystallographic order. The produced as-spun aliphatic aromatic copolyester fiber is an environmentally-friendly attractive, alternative to conventional chemical fibers for different applications.
 J Appl Polym Sci 119: 1896–1904, 2011

Key words: biodegradable; copolyester fibers; extrusion; rheology; X-ray; statistical modeling

INTRODUCTION

Biopolymers are biodegradable polymers based on either renewable or synthetic sources,[1] they break down in a short space of time in the natural environment. The production of novel and biodegradable fibers from biomass feed stocks has been facilitated by biotechnology used to produce the biopolymers. The use of composite materials is increasing at more than 10% per year; and bio-based materials will play a major role as environmentally friendly materials. In the last 25 years the world-wide production of petroleum source plastics has increased, and many governments have established laws to encourage recycling and use of bio-based environmentally friendly products to confront the problem of waste.[2]

Aliphatic–aromatic copolyesters are fully biodegradable petroleum polymers with stable physical and chemical properties and with comparable cost to other plastic polymers.[3] In an active microbial environment, the copolyesters products become invisible to the naked eye within 12 weeks.[4,5] Scientists have tried to improve the properties of bioplastics without affecting their biodegradability.[6] The biodegradability of polymers is influenced by the chemical structure of the polymer chains, crystallinity, chain orientation, and other morphological properties.[7] Although the degree of crystallinity is an important factor in determining microbial degradability, the biological resistance of the copolyesters is significantly influenced by the chemical structure.[8] Recently, there has been an increasing interest in applying biodegradable aliphatic/aromatic multiblock copolyesters for biomedical and nonwoven applications[9–13].

Extrusion temperature profile affects properties, productivity, and product cost.[14] One of the most important properties for the quality control of polymers is melt flow index (MFI): higher MFI leads to lower resin velocity and molar mass.[15]

Under processing, the viscoelastic nature of polymeric fluids has many complex effects on the flow stability.[16] Other properties such as molecular mobility and dye-ability of produced synthetic fibers are reduced by high orientation.[17,18]

Modern statistical experimental design methods help to produce the most satisfactory properties in the product for different applications; it has its difficulties as well as its usefulness. Statistical experimental design (SED) is still limited because of poor

Correspondence to: A. Fotheringham (a.f.fotheringham@hw.ac.uk).

attitude toward the statistical experimental design strategies and lack of collaboration between academic and industrial fraternities.[19] SED analysis solves the problems that rise in traditional analyses depending on the one factor at a time method.[20] It has the advantages of a one-step overall design in the development of process technology with known levels of confidence model. An achieved forecasting model specifies the direction of change of studied factors for increasing or reducing enhanced responses. In the melt spinning process many factors can be studied such as temperature profile, screw speed, metering pump speed, cooling system speed, and winding-up speed. For fiber work, preexperimental work should be carried out to find out the rheological data for determining the enhanced melt spinning conditions. As-spun AAC fibers were spun at different extrusion temperature profiles. Comparing the half-height widths of an X-ray scattering profile directly draws conclusions about the relative crystallographic order within a series of fibers.

FACTORIAL EXPERIMENTAL DESIGN

Experimental design analysis gives information about the significant main factors and the effects interactions through optimization of the average response value and depending on the factors and their levels.[21,22] First, some preexperimental work must be carried out to determine the number and the levels of factors, and to prepare the matrix design and the number of trials. After this process and the testing of the samples, the data are analyzed and the significant factors are determined to develop the process design.[23] Because the unsuspected factor's change with time may distort the analysis and result in misleading conclusions,[24] random errors could be separately distributed. There are many tools used in the statistical analysis of experimental design such as the Pareto chart, the effect plot, normal probability plot, surface plot, interaction plot, and analysis of variation (ANOVA). The theoretical basics about these tools will be described later with the results analysis. The programs used to obtain the matrix design and the statistical analysis plots are MINITAB[22] and STATGRAPHICS.[25]

THEORETICAL CONSIDERATIONS OF X-RAY DIFFRACTION (XRD)

X-ray diffraction is used to determine the sample crystalline spatial arrangement of the atoms within crystalline materials and to establish standards for assessing crystal structure and crystallinity.[26] Full-Width Half-Maximum (FWHM)[27,28] of an X-ray scattering profile is a function of the internal strain state in the investigated material. FWHM is an indication of degree of order of fiber structure developed during crystallization. According to the Debye-Scherrer formula [eq. (1)] the lower value of FWHM, the higher degree of crystallographic order and vice versa[29]:

$$t = K\lambda/B\ \mathrm{Cos}\theta \quad (1)$$

Where t is the averaged dimension of the crystallite, K is the crystallite shape constant, λ is the wavelength of the X-ray source, θ is the Bragg diffraction angle in degrees, and B is the diffraction peak width proportional to FWHM. Thus, K is assumed to be the same among all the fibers for which FWHM is determined. As the grade and the temperature profiles change, the fiber structure is expected to change and that will be seen in the intensity and the width of the crystalline peaks of X-ray diffraction traces. In X-ray diffraction traces, the crystallographic order degree increases with increase in the intensity of crystalline peaks, decrease in peak width and decrease in background area of scattering profile. A higher size of crystallite and the higher degree of crystallographic order are reflected qualitatively in a decrease in FWHM value of (110) planes and vice versa. Dramatically for all trials, the analysis will explain the gradually change in the factors and the structure obtained.

EXPERIMENTAL WORK

Materials

A fully biodegradable petroleum aromatic–aliphatic copolyester (AAC) (Solanyl flexibility component), based on butanediol, adipic acid, and terephthalic acid, supplied by Rodenburg Company, Netherlands, was used in this study. In terms of structure development, two grades of linear AAC (AAC1 and AAC2) were used in this stage. They are coded as MFI1 and MFI2 depending on their melt flow index MFI (Fig. 1). The material is referred to[30] as: 1,4-benzenedicarboxylic acid polymer with 1,4-butanediol and hexanedioic acid. The polymer shape is a spherical granule resin of diameter 3–5 mm with density of 1.22 g cm^{-3}. The range of melting temperatures is 110–115°C. Because of the low water solubility and high molar mass of the polymer ($>10^5$), it is unlikely to bio-accumulate.[31] No eco-toxicity data were submitted[32] and no significant toxicological effect was observed.[33] AAC meets the requirement of German standard DIN V 54900. Both of the AACs were dried at 60°C for 6 h before use, to avoid possible hydrolysis during the extrusion process.

Methods

Characterization of scattering traces

Wide angle X-ray scattering (WAXS) traces were obtained by using a Bruker D8Discover transmission

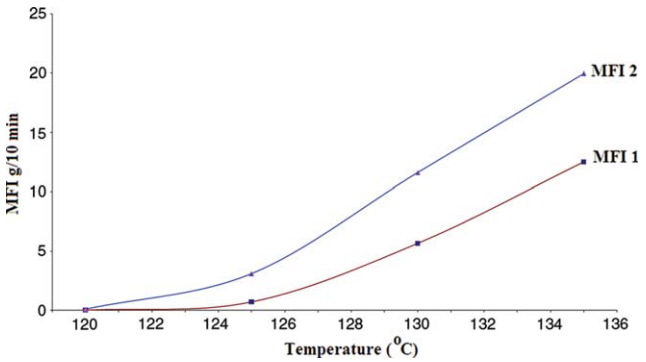

Figure 1 The relationship between MFI and temperature (AAC1 and AAC2 at weight = 2.16 kg). [Color figure can be viewed in the online issue, which is available at wileyonlinelibrary.com.]

X-ray diffractometer. A flat disk sample made by compacting tiny 1-mm lengths of fibers into a small 10-mm transparent holder was used; the detector is beneath the holder. The Discover uses a copper k-alpha target and transmits X-rays through the sample; the scan range was 15–28 (2θ°). When the X-ray source moves theta degrees (θ°), the detector stays in conjunction with it by 2 theta degrees (2θ°) throughout the scan. Full-width half-maximum (FWHM)[27,28] of (110) planes were calculated and processed digitally through DIFFRAC plus EVA computer programme.

Differential scanning calorimetry (DSC) characterization

A METTLER-TA Instrument DSC12E and METTLER-TOLEDO-TA89E System Software[34–36] was used to determine the thermal curves of 5- to 10-mg samples of AAC polymer and fibers. The weight values of the specimen were measured using three decimal places scale. Sample's aluminum pan was used in atmosphere of nitrogen; three replicates were scanned for each sample.

Melt flow index—MFI

Ray-Ran 5 Series Advanced Melt Flow Systems according to ASTM D-1238 was used to measure the melt flow index. The instrument contains a barrel with a standard die and piston. Granules of AAC are loaded into a heater block and left for 10 min to melt (ASTM D-1238) and condition to the right temperature. A fixed pressure was applied to the melt via a 2.16-kg loaded piston at different temperatures of 120, 125, 130, and 135°C.

Melt spinning

Fibers were extruded via melt spinning on a Lab-spin machine, Extrusion Systems Limited, UK,

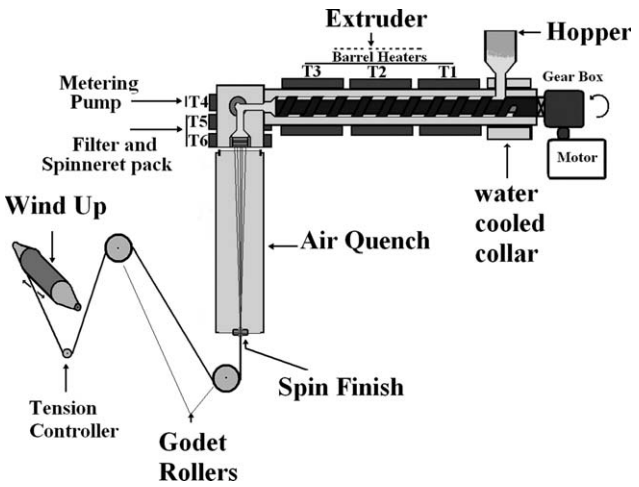

Figure 2 Schematic diagram of the melt spinning equipment.

shown in Figure 2. The Lab-spin machine consists of an extruder, a metering pump, a die head, an air cooling window, a spin finish application system, and a winding system. The temperature zones in the extruder are barrel zones (T1, T2 and T3), metering pump zone (T4), and die head zones (T5 and T6). Polymer granules are fed through the hopper into the extruder, then mechanically compressed and melted. The molten polymer is forced through the spinneret (55 holes) as fine jets with speed adjusted by the metering pump (fixed at 4 rpm) which generates the high pressure during metering. The air cooling quench speed was set at 37% of total blower fan air output. The filaments then cool down and harden progressively to emerge as solid filaments. The spin finish (Vickers) was diluted five fold with water before use with application speed of 0.4 rpm. The filaments were collected from the godets set at 36 m min^{-1} without tension between them and the winder (Fig. 2).

RESULTS AND DISCUSSION

Experimental design and results

The extrusion experiments conducted involved four factors at two levels, as given in Table I. The selected control factors covered the polymer grades

TABLE I
Factors and Their Levels for the Experiments (Temperature Values, °C)

	Factor						
	Z1		Z2		Z3		
Level	T1	T2	T3	T4	T5	T6	MFI
−1 (Low)	110	115	120	125	130	130	MFI 1
1 (High)	115	120	125	130	145	145	MFI 2

TABLE II
Experimental Array and the Experimental Results

Trial number	Block	MFI	Z1	Z2	Z3	FWHM
1	1	−1	1	1	1	0.630
2	1	−1	−1	−1	1	0.628
3	2	1	1	−1	1	0.579
4	2	1	1	1	−1	0.597
5	1	−1	1	−1	−1	0.590
6	2	1	−1	−1	−1	0.602
7	1	−1	−1	1	−1	0.621
8	2	1	−1	1	1	0.606
9	1	−1	1	−1	1	0.652
10	2	1	1	1	1	0.646
11	2	1	−1	−1	1	0.596
12	1	−1	−1	−1	−1	0.615
13	2	1	1	−1	−1	0.602
14	2	1	−1	1	−1	0.591
15	1	−1	−1	1	1	0.639
16	1	−1	1	1	−1	0.607

(MFI) and the extruder temperature zones. Two grades of linear AAC (AAC1 and AAC2) were used in this work; they are coded as MFI1 and MFI2 depending on their measured melt flow index MFI and it does not present the properties of the polymer fully. The temperature zones in the extruder are barrel zones (feeding zone temperature T1, compression zone temperature T2, metering zone temperature T3, metering pump temperature T4, and die head zones' temperature T5 and T6). To simplify the experiment, each two zones were combined and considered as one, i.e., Z1 = T1 + T2, Z2 = T3 + T4, and Z3 = T5 + T6. Depending on related work on the Brabender machine, the six temperature zones are condensed into three zones to decrease the unstable flowing because of viscosity and temperature interaction. That is because of the continuous flowing of the molten polymer between the die head zones (T5 + T6) and the heat diffusion between the metering zone of the screw (T3) and the metering pump (T4) which could not be controlled separately. In addition to that justification allowed keeping the temperature profile increasing from the screw feeding zone until the die head. That because polymers are bad conductors of heat and would need more time to cool down, that make a decrease in the temperature from zone to another is not possible. The experiments were conducted in two blocks for the polymer grade (MFI) because of the difficulty of cleaning the machine after each run. A fraction factorial experimental design (L16) for a simple experiment of four factors at two levels with random order was used as shown in Table II designed using STATGRAPHICS[25] software. The generated matrix (L16) clusters all experimental conditions to be controlled, as all factors levels appear the same number of times in each column, and allows all individual factors and their interactions to be analyzed statistically and evaluated independently.

Detailed comparisons of each trace reveal that some traces are more similar for each other than to others with slightly significant differences including the overall shape, the numbers and the positions of peak. In Figure 3(a) which presents typical X-ray diffractometer traces for the first block (lower MFI), there are five major crystalline diffraction peaks with different full-width half-maximum (FWHM) of an X-ray scattering profile observed at $2\theta^\circ = 16$, 17.5, 20.5, 23, and 24.5. In Figure 3(b) which presents typical X-ray diffractometer traces for second block (higher MFI), the same previous noted five peaks and an additional peak at $2\theta^\circ = 21.5$ were observed. The gradual structural change is attributed to the special features of the polymer grade and the extrusion temperature profile. The peaks observed at $2\theta^\circ = 16$, 20.5, 21.5, and 24.5 are very wide and weak. The peaks at $2\theta^\circ = 20.5$ and 23 are slightly sharper, more intense and smaller in width. The peak at $2\theta^\circ = 23$ was fitted using DIFFRAC plus EVA software to compare the half-height widths. From it, conclusions were drawn about the relative crystallographic order within a series of the 16 samples. FWHM results of the sixteen trials are listed in Table II; results analysis helps in evaluation of the effect

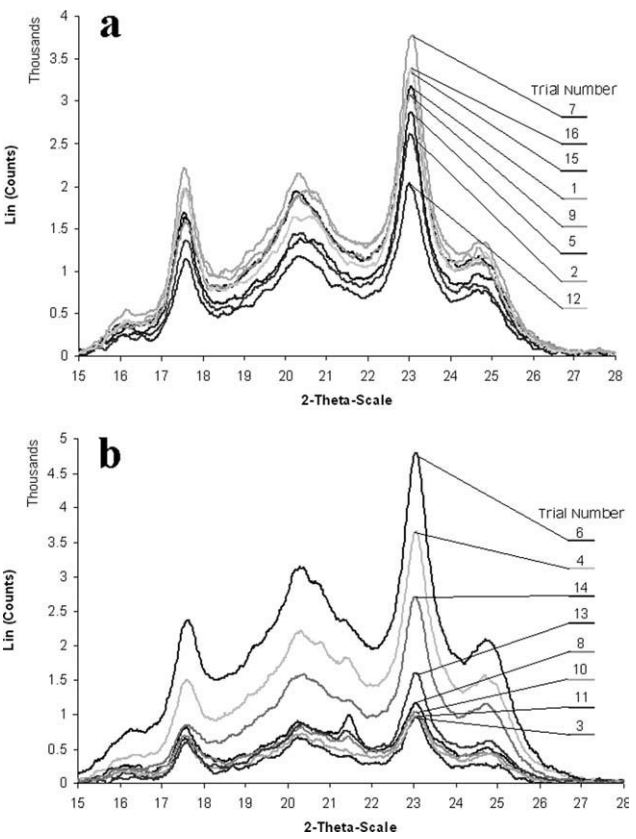

Figure 3 WAXS traces of AAC fibers for first (a) and second (b) blocks.

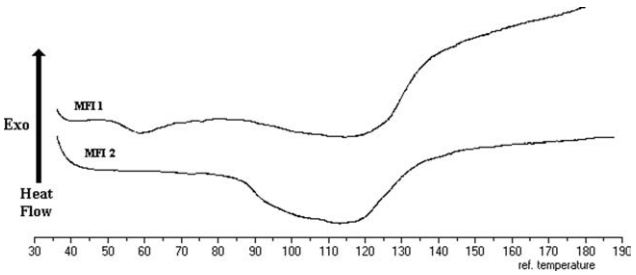

Figure 4 Thermal diagram of AAC.

between as-spun fiber structure and the drawability to enhance better drawn fibers. An increase in structure order is obtained in an increase in the peak intensity, a decrease in the peak width and a decrease in the background area. Such a quantification of structure order as a response parameter makes it possible to conduct systematic analysis of the polymer grade and the temperature profile on the fiber structure. This in turn will facilitate optimization and modeling of overall process.

In thermal diagrams of two AAC grades, Figure 4, a broad temperature range of melting (about 100–135°C) was observed for the polymer samples. According to the DSC results, an optimum temperature window was found taking all factors into account because the polymer does not melt completely below 120°C. The overall thermal behavior of the AAC polymer used in this work allows the conclusion that the processing window is quite wide. Therefore, the copolyester can be safely melt processed at 125°C.

In Figure 5, no appreciable changes of relative intensity of the peaks in the endotherm are observed in the fibers; the multiple melting phenomena observed could be attributed to compositional heterogeneity of the copolyester. Based on this fact, it can be suggested that AAC is a mixture composed of a number of components with different melting points. The endothermic curves of fractions are indicating that they are in the amorphous states. Ko et al.[37] relate the complex melting behavior as a result of the melting of different populations of lamellar crystals and/or the melting-recrystallization-remelting processes.

Statistical analysis of the effects of extrusion temperature profile and polymer grade on the FWHM

As a two-level experiment, a factor effect and interaction effect could be determined as the difference between the average responses at the low and the high level of the extrusion temperature profile zones and polymer grade. A Pareto chart for FWHM, Figure 6, shows the significant arrangement of factors and their interactions in decreasing order (y-axis) depending on the significant effect (x-axis). The decreasing order is MFI > Z3 ≫ MFI and Z3 > Z2 > Z1 and Z3 > Z2 and Z3 > MFI and Z1 > MFI and Z2 > Z1 and Z2 ≫ Z1.

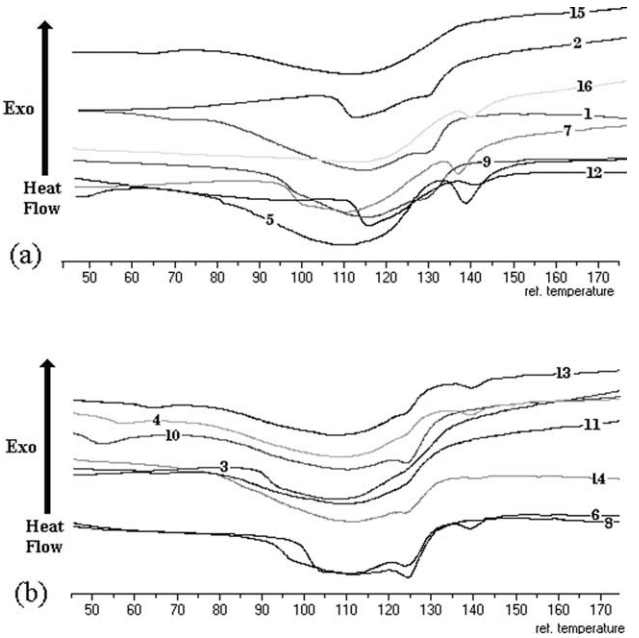

Figure 5 Thermal diagrams of fibers for first (a) and second (b) blocks.

Figure 7 shows the main effects and interaction plots of the statistical analysis of the effects caused by the main factors and their interactions on FWHM. In the effect plot, Figure 7(a), the factor effect between the average responses of the low and high level of the factors are presented, the capital letters along the horizontal axis representing the main factors. The effect line determines the effect of the factors from the length and the slope of the line between the two levels. The longer the effect line the more significant the factor effect. The direction of the effect is determined by the slope of the line: a positive effect is obtained when the line increases

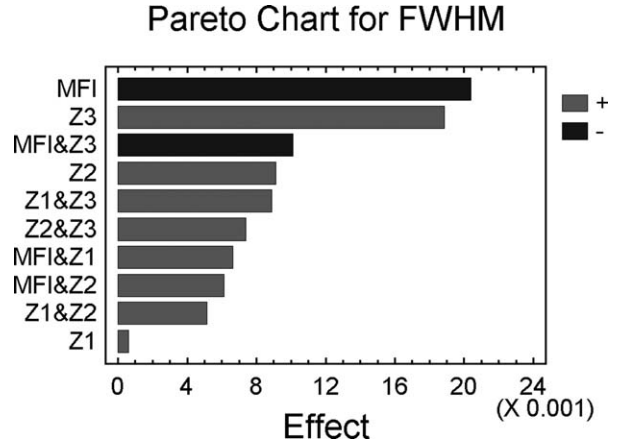

Figure 6 A ranked list of significant arrangement effects and interactions for FWHM (Pareto chart).

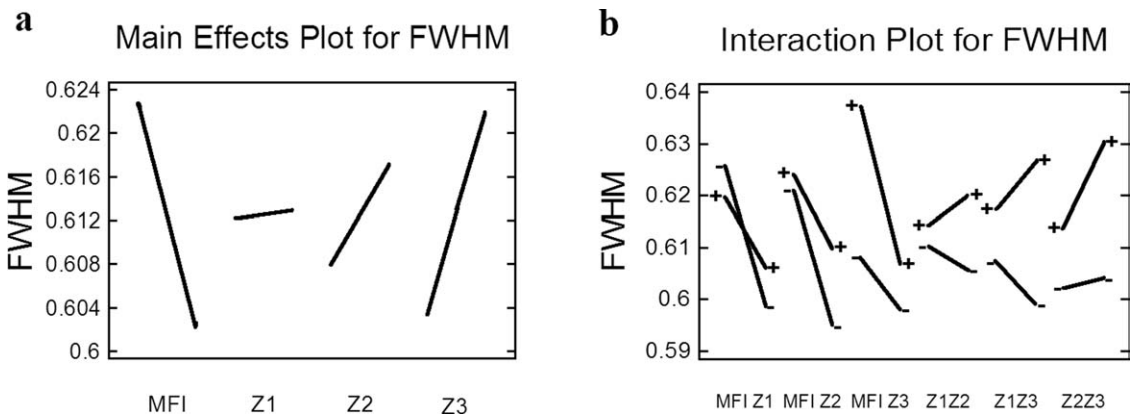

Figure 7 The effect and interaction plots for the response the FWHM, (a) and (b) are for the main factors and their interaction, respectively.

from the left to the right and vice versa. The main effects of MFI and Z3 (T5 + T6) are more pronounced than the other factors, Z1 and Z2, as their lines are longer and their slope is sharper than that of the other factors. FWHM increases either by increasing the temperature of the die head or by using the lower melt-flow index grade. In other words, increasing the temperature of die head or using the lower melt-flow index grade decreases the degree of crystallographic order.

To determine the form of the interaction between each two factors together and how the direction of change of the interacting factors influences the change on FWHM, an interaction plot is needed. In Figure 7(b), all the interactions could be simulated as the plot shows the existence or otherwise of each two factors interaction. For example, the interaction between MFI and Z3 is presented as MFIZ3 on the plot. The first factor (polymer grade coded as MFI) is presented on the x-axis from low level to high level, the second factor (die head temperature coded as Z3) shows as two different lines, one for low level coded as − and another for high level coded as +. The nonparallel lines confirm the presence of intersection. The y-axis shows the averages of the measured response, FWHM. It is a useful method to render the interaction between the polymer grade (MFI) and the die head temperature (Z3) relatively easy to understand, when the high level of die head temperature is paired with the lower MFI grade, the maximum FWHM (or lower degree of crystallographic) is obtained. However, there are two noteworthy interactions, MFIZ3 and Z1Z3; their significance should be investigated because of the small angles between the interaction lines. The major factors influencing FWHM value would be advised to be assessed further to understand their influence more fully. The small effect of Z2 and its interaction with Z3 are related to the heat diffusion between the metering pump and die head as a result of the continuous flowing of the molten polymer.

STATGRAPHICS[25] is used to calculate statistical standardized and percentage order factors and their interactions values, then to plot them on x and y axes, respectively, to generate a normal probability plot or a Daniel's plot. This technique helps in the separation process of factors into important/unimportant categories and gives more details whether the factor's effect is positive or negative.[38] The straight line represents the empirical principle in the middle of the range; the significant effect for both positive and negative effect could be reflected in deviation of the data points from the straight line. The further the deviation, the greater the statistical significance. If responses follow a normal distribution pattern, there are no statistically significant factor effects in the experiment. Figure 8 displays the normal probability plot of the derived effect estimated and gives more details about the normal distribution for the data. The effects from MFI and Z3 and their interaction are again prominent; the effects from Z1, Z2, and other interaction are less

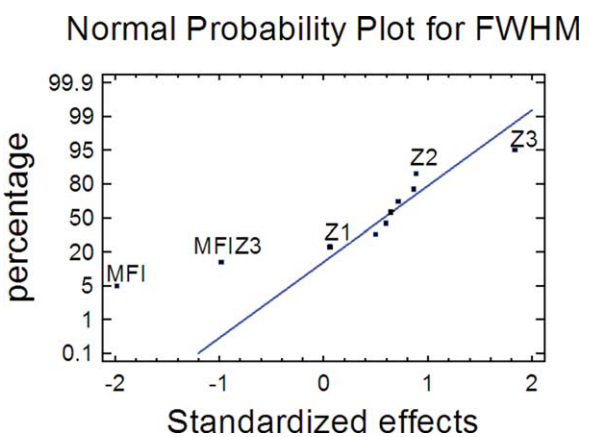

Figure 8 Statistical standardized and percentage order values of factors and their interactions for the FWHM (Normal Probability Plot). [Color figure can be viewed in the online issue, which is available at wileyonlinelibrary.com.]

TABLE III
Results from Analysis of Variance (ANOVA) of the Data Identifying the Statistical Significance of Factor

Source	Sum of squares	Degrees of freedom	Mean square	*F*-ratio	*P*-value
MFI	0.00166056	1	0.00166056	5.94	0.0330
Z2	0.000333063	1	0.000333063	1.19	0.2985
Z3	0.00142506	1	0.00142506	5.09	0.0453
MFI Z3	0.000410063	1	0.000410063	1.47	0.2514
Total error	0.00307563	10	0.000307563		
Total (corr.)	0.00690594		15		

prominent. More details about the effect significance will be obtained from ANOVA for FWHM.

Analysis of variance (ANOVA) for FWHM

To determine the factor effects in terms of statistical significance, analysis of variance (ANOVA) of the data was conducted. The ANOVA method designed by Sir R. A. Fisher[21] is a mathematical method: it compares the response data to the error data, to determine the significant effect of the independent factors or from their interaction.

ANOVA depends on the *F* test, the *F*-ratio being obtained from statistical *F* tables at the appropriate level $\alpha = 0.05$.[20–22] If the *F* value is greater than the critical *F* value, $F = 4.96$ in our work, its factor has a significant effect on the response. After calculating the *F* value, the *P* value is determined using the graphic method ($P \equiv \alpha$-significance level) and can be obtained from most modern statistical analysis programs. A probability or *P*-value used in ANOVA provides quantitative and objective criteria for judging the statistical significance of the effects. Each factor has a *P*-value less than 0.05 indicates that the factor is significantly different from zero at the 95.0% confidence level. An error could come from either assignable causes that represent variation due to changes in the independent factors, or random causes that signify uncontrolled variation.

The ANOVA table partitions the variability in FWHM into separate parts for each effect, and then tests the statistical significance of each effect by comparing the mean square against the experimental error. The results are listed in Table III. The significance of the studied factors will then be MFI (0.0330) > Z3 (0.0453). Even there is prominent interaction between MFI and Z3 as mentioned before, its *P*-value (0.2514) is bigger than 0.05. As a result, the interaction MFI and Z3 has no significant effect. There are no significant effects of the other interactions within the temperature range in the experiments.

The regression equation and estimation results for FWHM

The pattern of estimated responses is based on the assumed model derived from the experimental observations. The geometric result of plotting a response variable is as a function of two factors and the interaction appears with the surface twist. To determine the direction of the interaction MFIZ3, the estimated response surfaces of FWHM is used as shown in Figure 9. There are three axes, the first factor MFI is on the *x* axis with low and high levels, the second factor Z3 is on the *y* axis with low and high levels, and *z* axis shows the averages of the measured MFIZ3. The estimated response surface is based on the assumed regression model. As the surface is flat with no twist found in the surface, no significant effect has been detected between MFI and Z3. And that agrees with the previous statistical analysis results of the interaction plot and ANOVA derived from the experimental data.

Based on the analysis of the fraction factorial experimental design (L16) results and using STATGRAPHICS program, simplified model was fitted by the regression equation [eq. (2)], which has been fitted to the experimental data. The regression equation in terms of the previous coded values in Table I is the following:

$$\begin{aligned}\mathbf{FWHM} = {} & 0.612562 - 0.0101875 * \mathrm{MFI} \\ & + 0.0003125 * Z1 + 0.0045625 * Z2 + 0.0094375 * Z3 \\ & + 0.0033125 * \mathrm{MFI} * Z1 + 0.0030625 * \mathrm{MFI} * Z2 \\ & - 0.0050625 * \mathrm{MFI} * Z3 + 0.0025625 * Z1 * Z2 \\ & + 0.0044375 * Z1 * Z3 + 0.0036875 * Z2 * Z3 \quad (2)\end{aligned}$$

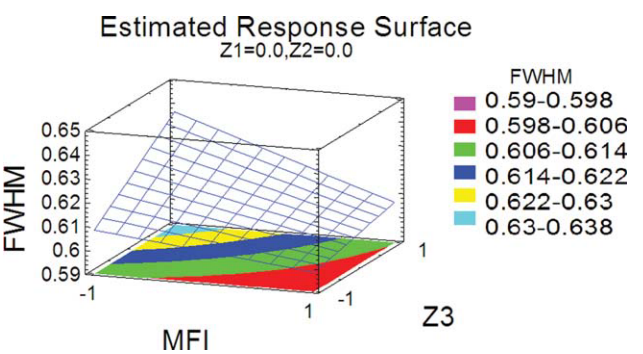

Figure 9 The FWHM Estimated response surface for the interaction between MFI and Z3. [Color figure can be viewed in the online issue, which is available at wileyonlinelibrary.com.]

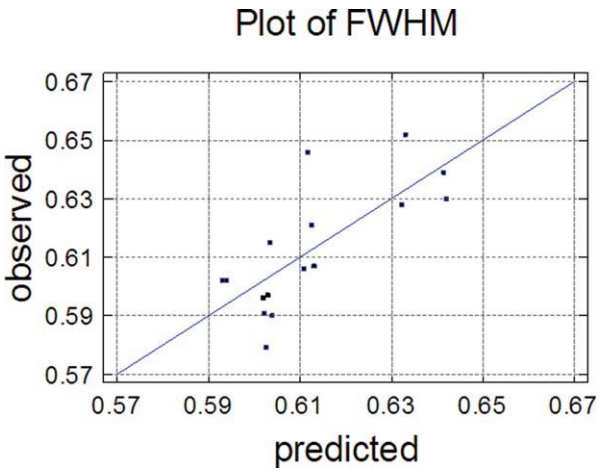

Figure 10 Experimental observed results and theoretical fitted results plot for FWHM. [Color figure can be viewed in the online issue, which is available at wileyonlinelibrary.com.]

The model evaluates the significance effect of each independent variable to a predicted response depending on the coefficient constant for the linear effects of independent factors and the coefficient constant for the interactions effects, where 0.612562 is coefficient constant for offset term.

Figure 10 shows the Experimental observed results and theoretical fitted results plot of FWHM. Experimentally observed results are plotted on the y axis, and FWHM for theoretical fitted results generated using the last fitted model is plotted on the x axis for each trial. The predicting model gave acceptable results with small variation (0.02) for reasons such as: (i) blocked nozzles in the spinneret because of the nature of this polymer and the nonuniform flow, (ii) the tension, (iii) some tension during preparing the sample for the test or (iv). The interaction Z2Z3 effect is related to the heat diffusion between the metering pump and die head as a result of the continuous flowing of the molten polymer.

Square and cube plots are used to summarize predicted values for the dependent variable by giving the respective high and low setting of factors. The cube plot shows the predicted values for three factors at a time, the square plot shows the predicted values for two factors at a time.

In Figure 11(a) and depending on the regression equation, each value corresponds to the values of the experimental factors Z2, Z3, and MFI at the middle level of Z1 range (between −1 and + 1) that is 0. In Figure 11(b), the square plot gives more details about the relationship between Z3 and MFI at the middle levels of both Z1 (0) and Z3 (0) ranges.

In conclusion, there are two significant factors affecting the crystallographic order which are the AACs grade used and the die head temperature (Z3) at which the polymer melt passes through the spinneret.

CONCLUSIONS AND STATISTICAL MODEL FOR OPTIMIZATION

A production process for biodegradable fiber has been developed from linear aliphatic–aromatic copolyester. Based on DSC and XRD data, the tow grades used show differences in crystallization and rheological behaviors. In term of characterization of individual polymer grade, the analyzed data shows that the temperature of the die head should be considered. There are interactions between temperature zones related to the heat diffusion between barrel zones, the metering pump and die head as a result of the continuous flowing of the molten polymer. In the optimization of full-width half-maximum of an X-ray scattering profile (FWHM), Table IV shows the combination of factor levels which maximize and minimize FWHM over the indicated region. The lower value of FWHM leads to the higher size of the

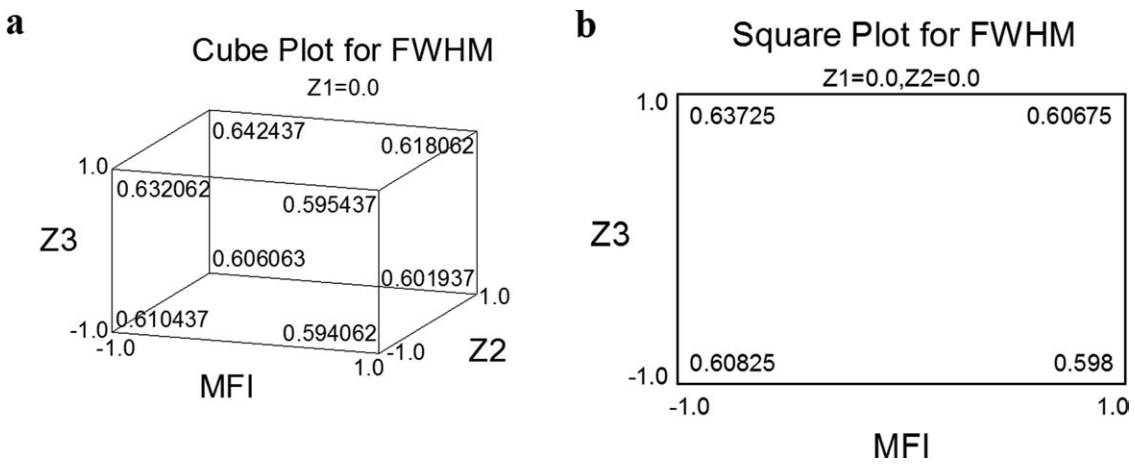

Figure 11 FWHM Cube (MFI, Z2 and Z3, a) and Square (MFI and Z3, b) plots of the estimated effects for the high and low studied factor settings.

TABLE IV
The Combination of Factor Levels Which Maximize and Minimize FWHM Over the Indicated Region

	Maximum FWHM value (lower degree of crystallographic)		Minimum FWHM value (higher degree of crystallographic)	
Optimum value	0.646437		0.589937	
Factor	Optimum model	Actual value	Optimum model	Actual value
MFI	Low level	MFI 1	High level	MFI 2
Z1	High level	115–120	Low level	110–115
Z2	High level	125–130	Low level	120–125
Z3	High level	145–145	High level	145–145

crystallite and the higher degree of crystallographic order and vice versa. The statistical model covers the polymer grade, extruder zone temperatures, and their interactions and specifies the combinations of their levels for enhancing crystallographic order. With previous work[39,40] on overall orientation, current results assist the understanding of the processing of AAC fibers. A grade with lower melt flow index should be selected for future work on extrusion process modeling. The model helps processing scientists and technologists in industry to obtain the enhanced crystallographic order at suitable conditions related to final product cost to get environmentally friendly, economical, energy saved fibers. Mechanical properties will be investigated in future work.

The authors are indebted to Dr. Robert. R Mather, Heriot-Watt University, School of Engineering and Physical Sciences (EPS), for helpful comments and stimulating discussions and to Mrs. M. K. Millar, Heriot Watt University, EPS, for the technical support on the X-ray diffractometer.

References

1. Blackburn, R. S. Biodegradable and Sustainable Fibres; The Textile Institute: USA, 1997.
2. Chandra, R.; Rustgi, R. Biodegradable Biopolymers; Elsevier Science: Great Britain, 1998.
3. Fang, Q.; Hanna, M. A. Bioresour Technol 2001, 78, 115.
4. Environment Australia, Biodegradable Plastics—Developments and Environmental Impacts, NOLAN-ITU Pty Ltd, Australia 2002.
5. Witt, U.; Muller, R.-J.; Deckwer, W.-D. J Polym Environ 1995, 3, 215.
6. Stevens, E. S. Green Plastics; Princeton & Oxford: UK, 2002.
7. Ki, H. C.; Park, O. O. Polymer 2001, 42, 1849.
8. Okada, M. Prog Polym Sci 2001, 27, 87.
9. Lu, F.; Ahaile, W.; Etincher, M.; Wiley, S. H. The World Intellectual Property Organization (WIPO), 028626, 2002.
10. Twarowska-Schmidt, K.; Ratajska, M., Fibres Text East Eur 2005, 13, 71.
11. Seala, B. L.; Oterob, T. C.; Panitch, A. Mater Sci Eng 2001, 34, 147.
12. Renke-Gluszko, M.; Fray, M. E. Biomaterials 2004, 25, 5191.
13. Prowans, P.; Fray, M. E.; Slonecki, J. Biomaterials 2002, 23, 2973.
14. Capasso, V. Mathematical Modelling for Polymer Processing; Springer-Verlag: Berlin, 2003.
15. Giles, H. F.; Wagner, J. R.; Mount, E. M. Extrusion: The Definition Processing Guide and Hand Book; William Andrew: Norwich, 2005.
16. Aarts, A. C. T. Analysis of the Flow Instabilities in the Extrusion of Polymeric Melts: PhD Thesis, Eindhoven University of Technology, Eindhoven, The Netherlands, 1997.
17. Kadolph, S. J.; Langford, A. L., Textiles, 9th edition; Pearson Education Inc., New Jersey, USA, 2002.
18. Brody, H. Synthetic Fibre Materials; Longman Group UK Limited: London, 1994.
19. Antony, J.; Perry, D.; Wang, C.; Kumar, M. Assembly Automation 2006, 26, 18.
20. Phadke, M. S. Quality Engineering Using Robust Design; AT&T Bell Laboratories: USA, 1989.
21. Lochner, R. H.; Mater, J. E. Design for Quality; Chapman and Hall: London, 1990.
22. MINITAB. Minitab Inc: USA, 1994.
23. Cawse, J. N. Experimental Design for Combinatorial and High Throughput Materials Development; Wiley: USA, 2003.
24. Montgomery, D. C. Design and Analysis of Experiment; Wiley: New York, 1997.
25. STATGRAPHICS Plus Version 5.1, USA, 2001.
26. Warner, S. B. Fiber Science; Prentice-Hall: New Jersey, 1995.
27. Guinier, A. X-ray Diffraction: In Crystals, Imperfect Crystals, and Amorphous Bodies; Courier Dover: USA, 1994.
28. Berkum, J. G. M. V.; Dellhez, R.; keijser, T. H.; Mittemeijer, E. J. Diffraction-Line Broadening Analysis of Strain Fields, In Defect and Microstructure Analysis by Diffraction; Oxford University Press: Oxford, 1999.
29. Patterson, A. L. Am Phys Soc 1939, 56, 978.
30. National Industrial Chemicals Notification and Assessment Scheme (NICNAS): Australia, February 2003.
31. Connell, D. W. General Characteristics of Organic Compounds Which Exhibit Bioaccumulation, In Bioaccumulation of Xenobiotic Compounds; CRC Press: Boca Raton, USA, 1990.
32. Nabholz, J. V.; Miller, P.; Zeeman, M.; In Environmental Risk Assessment of the New Chemicals Under the Toxic Substances Control Act (TSCA) Section Five, Environmental Toxicology and Risk Assessment. ASTM STP 1179; Wayne G. L.; Jane, S. H.; Michael, A., Eds.; Lewis ASTM: Philadelphia, 1993.
33. Witt, U.; Einig, T.; Yamamoto, M.; Kleeberg, I.; Deckwer, W.-D.; Müller, R.-J. Chemosphere 2001, 44, 289.
34. METTLER. METTLER System software TA89E. METTLER -Toledo AG, Switzerland, 1990.
35. METTLER. METTLER TOLEDO TA89E System software VERSION 3. METTELER -Toledo AG, Switzerland, 1993.
36. METTLER TA Instrument DSC12E, METTLER -Toledo AG, Switzerland, 1990.
37. Ko, C.-Y.; Chen, M.; Wang, C.-L.; Wang, H.-C.; Chen, R.-Y.; Tseng, I.-M., Polymer 2007, 48, 2415.
38. Gardiner, W. P.; Gettinby, G. Experimental Design Techniques in Statistical Practice, A Practical Software-Based Approach; Horwood: England, 1998.
39. Younes, B.; Fotheringham, A.; EL-Dessouky, H. M. Polym Eng Sci 2009, 49, 2492.
40. Younes, B.; Fotheringham, A.; EL-Dessouky, H. M. J Appl Polym Sci, Early View (10.1002/app.32002), 2010.